Received: 1 August 2021 | Revised: 1 March 2022 | Accepted: 3 March 2022

DOI: 10.1002/esp.5359

RESEARCH ARTICLE

ESPL WILEY

Salt-marsh retreat on different time scales: Issues and prospects from a 5-year monitoring campaign in the Venice Lagoon

Riccardo A. Mel[1] | Michele Bendoni[2] | Daniele Steffinlongo[3]

[1]Department of Environmental Engineering, University of Calabria, Arcavacata di Rende, Italy

[2]LaMMA Consortium, Sesto Fiorentino, Italy

[3]Ordine degli Ingegneri della provincia di Venezia n° 4698, Venezia, Italy

Correspondence
Riccardo A. Mel, Department of Environmental Engineering, University of Calabria, via Pietro Bucci, 87036 Arcavacata di Rende (Cs), Italy.
Email: riccardo_alvise.mel@unical.it

Abstract

Lateral edge erosion is one of the main mechanisms leading to loss volume of salt marshes. Given the relatively large number of field measurements of eroding salt marshes reported in the literature, and the different ways they were performed, some natural questions arise. (i) What is the relationship between wave climate and erosion rate at different time scales? (ii) How can the surveys based on a single meteorological event support large-scale monitoring campaigns? (iii) What are the main meteorological and morphological parameters correlated to the erosion process? (iv) Why do only some marshes show cantilever profiles? (v) What are the most common issues to deal with in monitoring campaigns? Most of the previous studies considered large spatial and temporal scales only, providing an estimation of the overall behaviour of the system without identifying the specific role of each event. In this study, we attempted to answer these questions by investigating the lateral evolution of salt marsh margins located in the Venice Lagoon at different time scales, combining marsh retreat measurements, remote sensing data and numerical modelling. Field data were collected monthly for 5 years (2014–2018), covering 26 storms. A linear relation linking erosion rate to wave power is confirmed at different time scales, with a decreasing slope at higher elevation of the marsh bank that explains the occurrence of cantilever profiles. Mass failures can occur over long-period cycles, related to the geomorphic characteristics of the area. Finally, the major issues affecting the *in-situ* monitoring campaigns have been highlighted.

KEYWORDS
field monitoring, lateral retreat, morphodynamics, remote sensing, salt marshes, Venice Lagoon, wind climate

1 | INTRODUCTION

Salt marshes are geomorphic landforms characterizing intertidal environments such as lagoons and estuaries (Boicourt, 1993; Luternauer et al., 1995; Mitsch & Gosselink, 2000; Rogers & Woodroffe, 2014). Physical, biological, and chemical processes interact, giving rise to complex dynamical interactions. Salt marshes provide multiple ecosystem services to the environment, supporting the biodiversity, primary production, water purification, carbon sequestration, and providing protection from extreme storms (Barbier et al., 2011; Bouma et al., 2014; Costanza et al., 1997; Craft et al., 2008; Fagherazzi et al., 2020; Fourqurean et al., 2012; Howes et al., 2010; Möller et al., 2014; Temmerman et al., 2013). The morphologic evolution of tidal marshes can be explained as a delicate balance between the processes supporting marsh expansion (e.g. vertical accretion and vegetation colonization) and those endangering it, such as surface and margin erosion. Rate of relative sea level rise (RSLR), tidal regime, wind-wave climate, sediment supply, development of a vegetation

cover related to RSLR, and temperature trend are fundamental driving forces for the morphologic evolution of salt marshes (Silvestri & Marani, 2004; Evans et al., 2019, 2021). Nowadays, shallow-water environments are experiencing dramatic morphological and ecological degradation due to increasing anthropic pressure, RSLR, and erosive processes, intensified by a decrease in sediment supply (Fagherazzi et al., 2013; Mariotti & Fagherazzi, 2013). Several marshes are currently subject to far-reaching irreversible transformation, with social, economic, and ecological implications (D'Alpaos et al., 2011; FitzGerald & Hughes, 2019; Gedan et al., 2009; Ratliff et al., 2015).

Environmental degradation is particularly prominent in the Venice Lagoon, Italy. Few other areas in the world have experienced such an enduring and profound interplay between human action and biophysical dynamics over the years. Over the centuries, the Republic of Venice has constantly considered the integrity and preservation of the lagoon as fundamental (Deheyn & Shaffer, 2007). However, in the last century, attention on the health of the lagoon has partially diminished. The construction of jetties at the inlets, excavation of large navigable channels, natural and human-induced subsidence, RSLR, boat wave erosion, and the lack of riverine sediment supply have significantly changed the morphology of the lagoon, affecting its hydrodynamic regime and leading to the loss of large portions of salt marshes (Carniello et al., 2009; D'Alpaos & Martini, 2005; Deheyn & Shaffer, 2007; Sorokin et al., 2002; Tambroni & Seminara, 2006; Tommasini et al., 2019). Several geomorphological investigations performed in the Venice Lagoon pointed to a significant retreat of the salt marshes, mainly caused by human interventions (e.g. dredging for navigation, building hard structures for sea defence, land reclamation). The current scenario is a negative sediment budget, which produces significant morphological transformations (Carniello et al., 2009; Ghinassi et al., 2018), driving the lagoon to a generalized bottom deepening. The total net sediment loss between 1927 and 2002 reached 110 Mm^3 (Sarretta et al., 2010), affecting both salt marsh areas, which decreased from 170 km^2 (1901) to about 43 km^2 (2012), and the depth of the tidal flats, triggering further erosion processes (Tommasini et al., 2019). The retreat of salt marshes and the deepening of tidal flats increased fetch distances and mean water depth, allowing winds to generate higher waves, which in turn enhance the erosion processes through a positive feedback mechanism that is still ongoing (Finotello et al., 2020; Mariotti & Fagherazzi, 2013).

As an endmember of a series of nested systems which interact non-linearly (Global Earth, Atlantic Ocean, Mediterranean Sea, Adriatic Sea, Po coastal plain), the eco-morphological equilibrium of the Venice Lagoon is threatened by climate change, which can generate unpredictable effects. In addition, the local climate—such as air and water temperature, rain frequency, and RSLR—can be affected by land use and human activities (Findell et al., 2017). Though many local factors are still rather uncertain, the IPCC intermediate scenario (IPCC, 2013) shows that in future decades global warming would cause several morphologic and environmental transformations in the Venice Lagoon (Tagliapietra et al., 2011). In spite of these alarming trends, only recently have systematic monitoring campaigns focused on the erosive processes promoting marsh edge retreat been performed. In the last two decades, some physical and biological processes involving the evolution of salt marshes have begun to be studied more carefully: the development of wave cut gullies (Priestas & Fagherazzi, 2011), the effect of marsh vegetation (Feagin et al., 2009; Moller, 1999, 2006), the role of marsh morphology and composition (Bendoni et al., 2019; Evans et al., 2019; Schoutens et al., 2020) and sea level on scarp erosion (D'Alpaos et al., 2011; Mariotti et al., 2010; Tonelli et al., 2010). Wang et al. (2017) identified spatial scale-dependent factors affecting marsh edge erosion through a multiscale approach, linking the large-scale lateral retreat rate of the marsh to sediment erodibility at the local scale. Some authors (Gedan et al., 2009; Leonardi et al., 2016b; Priestas et al., 2015; Schwimmer, 2001) found a power-law relationship between erosion rate and wave forcing through estimation of edge retreat over a long time scale (order of decades). Marani et al. (2011) found that such a relationship is linear. Bendoni et al. (2016) carried out a field study in a salt marsh in the Venice Lagoon, obtaining a linear relation between erosion rate and wave forcing also at a monthly time scale. Long-term scales (order of months, years, or decades) can make the estimation of the erosion progressively more robust, but do not allow us to identify the role of specific events and only implicitly account for the characteristics of the local environment. A detailed description of the effects of the seasonality in wind-wave forcing is still not available, and lateral retreat rates are usually determined without providing any information about their inter-annual variability.

More efforts are needed to investigate marsh edge erosion at short time scales, to support and validate the findings based on longer time scales. Hydrodynamics in front of the scarp is crucial for the evolution of salt marshes, even more if climate variability is included in the analyses. The shape of the scarp and the vegetation of the marsh, together with the possible lateral migration of adjacent tidal channels, are relevant aspects, since they can trigger cantilever profiles and further mass failures (Bendoni et al., 2016; Finotello et al., 2018, 2020; Van Eerdt, 1985). It is usually assumed that cantilever profiles depend on the presence of a root mat reinforcing the bank in the upper part, leaving the toe more sensible to wave erosion. However, the temporal distribution of water level modulated by the tide in front of the bank and the wind fetch may play a decisive role in the geomorphic evolution of the scarp. In addition, the role of the angle of incidence of the waves in affecting the erosion process is not completely clear. Marani et al. (2011) proposed that the instantaneous incident wave power density is a function of the cosine of the angle between the marsh margin and the wave propagation direction, which is assumed coincident to the wind direction. On the one hand, waves approaching the bank orthogonal to the marsh boundary lead to wave impact; on the other hand, waves approaching the marsh boundary obliquely may have a shear and dragging effect on the bank material. Furthermore, some aspects potentially leading to significant errors in field measurements deserve to be identified and addressed by means of surveys performed after single meteorological events, combined with a continuous monitoring of the area.

In this study, we analysed a dataset collected in the Venice Lagoon from January 2014 to December 2018. Measurements of lateral retreat were collected yearly, monthly, and after 26 storm surges. We focused on the derivation of a functional relationship between wave climate modulated by tidal level (energy flux) and the erosion rate at different temporal scales (e.g. yearly, monthly, and for single meteorological events). Remote sensing data gauged during these meteorological events, combined with the implementation of the Young and Verhagen (1996) wave model, further improved by Breugem and Holthuijsen (2007), allowed us to estimate the wave

climate in front of the bank for the whole period 2014–2018. We performed a sensitivity analysis on the parameters involved in the erosion process (i.e. wave angle and marsh elevation) to identify the combination which best fits field data.

The paper is organized as follows. The next section describes the location and methodologies adopted for the measurement campaign. Lateral retreat and wind-wave data analysis, and the relation between wave power and erosion rate at different time scales, are presented in the third section. The fourth section includes a thorough discussion of the results. For each topic, we highlight the encountered issues, providing some tips to implement strategies that should be adopted in future monitoring campaigns. Sea levels are referred to the official 1892 local (i.e. Punta della Salute) reference datum for the Venice Lagoon, located about 0.3 m below the present mean sea level.

2 | MATERIALS AND METHODS

2.1 | Geomorphologic settings

The Venice Lagoon is a brackish water body extending for 550 km^2, oriented northeast–southwest, located in the northern part of the Adriatic Sea, to which it is connected by the Lido, Malamocco, and Chioggia inlets (Carniello et al., 2009). The Venice Lagoon originated during the Holocene transgression (Tosi et al., 2012; Zecchin et al., 2009) and nowadays consists of a group of islands, extensive tidal flats, and salt marshes mainly colonized by halophytic species, drained by intricate networks of branching and meandering tidal channels (Carniello et al., 2009; Cosma et al., 2019; Finotello et al., 2018; Ghinassi et al., 2018; Marani et al., 2006). The bottom is mainly composed of sand in the main channels branching from the three inlets (representative $D_{50} = 200$ μm), and cohesive sediments elsewhere (representative $D_{50} = 20$ μm) (Carniello et al., 2012; Molinaroli et al., 2009).

The tide is the main hydrodynamic driver for the transport of suspended material across the lagoon, with a mean tidal range from 0.5 m during neap tide to 1.0 m during spring tide (D'Alpaos et al., 2013). The tidal forcing affects the advection and dispersion of sediments, nutrients, and contaminants (Falcão et al., 2009), and the storm surge propagation into the lagoon. The mean water depth of the water body is about 1.5 m with respect to the present mean sea level and the mean elevation of the salt marshes is about 0.25 m above mean sea level (bathymetric data used in this study have been provided by the Venice Water Authority; see Carniello et al., 2009).

The monitored area comprises three alongshore edge transects of a salt marsh located in the northern part of the Venice Lagoon between Burano and Sant'Erasmo islands (Figure 1b). Our analysis focused on a naturally preserved marsh and the three transects are exposed to dominant wind direction (bora wind; see Mel et al., 2019). The range of the bora wind direction is 20–60°N, allowing us to study different angles of the waves approaching the scarp (Figure 1b).

We performed a grain size analysis of some sediment samples collected in the monitored marsh to investigate the soil composition at three different elevations within the bank (i.e. at the top, at the lower part of the scarp, and at the toe) (transect 2, Figure 1c). The representative size of the grains is $D_{50} = 0.3$ mm. It is slightly higher at the top, probably related to the larger amount of root biomass, as shown by Wang et al. (2017). Several species are present on the marsh surface. The most frequent are *Aster tripolium*, *Limbarda crithmoides*, *Limonium narbonense*, *Puccinellia palustris*, *Salicornia*, and *Suaeda maritima*. The surveyed area displays cantilever profiles and mass failure events.

2.2 | Lateral retreat measurements

Two parallel erosion measurements were carried out during the monitoring period (January 2014–December 2018) based on different time scales: red erosion pins were employed for the monthly and yearly analysis (Figure 2b); blue pins for single storm events (Figure 2d). In both cases erosion pins were placed horizontally, along the bank vertical face. The erosion has been computed as the lateral retreat for each pin with respect to the previous survey. When a mass failure occurred, the eroded length was set equal to the width of the failed block, and the pin was then reinserted in the marsh bank. The elevations of bank top, bank toe, and pin were determined through GPS measurements.

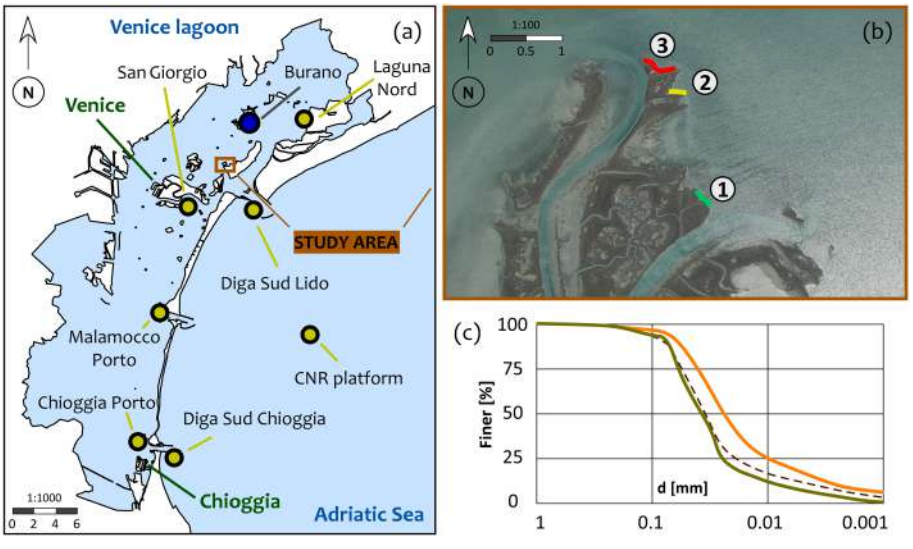

FIGURE 1 The Venice Lagoon and the marsh surveyed in this work. (a) Location of the study area and gauging network. (b) Location of the three surveyed transects. (c) Soil composition characterizing the surveyed salt marsh. Soil samples were collected at different elevations of the marsh scarp belonging to transect 2. Yellow line refers to the upper part of the marsh; orange line to the lower part; brown dashed line to the tidal flat immediately adjacent to the bank toe [Color figure can be viewed at wileyonlinelibrary.com]

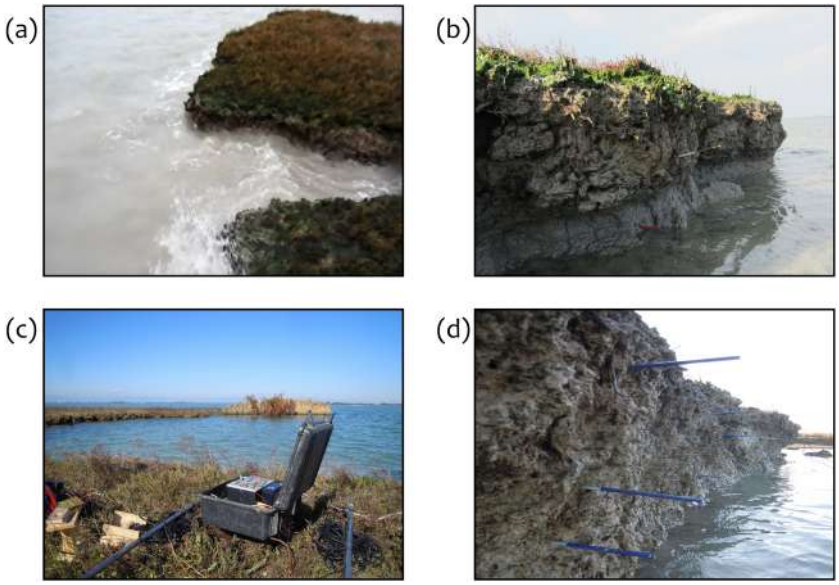

FIGURE 2 Salt marsh surveyed in this work. (a) Waves impinging the margin (transect 3). (b) Erosion pins used for the monthly and yearly surveys (transect 1). (c) Overview of the datalogger and pressure transducers used to measure the in-field wave climate (transect 2). (d) Erosion pins used for the single surge surveys (transect 2) [Color figure can be viewed at wileyonlinelibrary.com]

2.3 | Wind-wave climate

Erosion rates computed in the 26 single meteorological events were related to the wave power computed on the basis of the in-field measurements. Erosion rates computed at monthly and yearly time scale were related to wave power coming from the Young and Verhagen (1996) wave forecast model (further improved by Breugem & Holthuijsen, 2007), forced by wind and sea level dataset in the period 2014–2018, and properly adjusted on the basis of the wave climate data collected through remote sensing field measurements. Specifically, equations determining the offshore significant wave height H_{m0} and peak period T_p are

$$\frac{gH_{m0}}{U_w^2} = 0.24\left\{\tanh A_1 \tanh\left[\frac{B_1}{\tanh A_1}\right]\right\}^{0.572}$$

$$\frac{gT_p}{U_w} = 7.69\left\{\tanh A_2 \tanh\left[\frac{B_2}{\tanh A_2}\right]\right\}^{0.187}$$

where

$$A_1 = 0.343\left(\frac{gh}{U_w^2}\right)^{1.14}; B_1 = 4.41\cdot 10^{-4}\left(\frac{gF}{U_w^2}\right)^{0.79}$$

$$A_2 = 0.1\left(\frac{gh}{U_w^2}\right)^{2.01}; B_2 = 2.77\cdot 10^{-7}\left(\frac{gF}{U_w^2}\right)^{1.45}$$

and h, F, and U_w are the mean water depth, fetch length, and wind speed, respectively. Water depth and fetch are a function of the wind direction with respect to the marsh edge $\varphi(t)$. The water depth depends on the sea level η and on the bed level z_b:

$$h(t) = \eta(t) - z_b[\varphi(t)]$$

The fetch is determined through the relation proposed by Saville (1954):

$$F(\varphi_i) = \frac{\sum_{j=-45}^{45} F(\varphi_{i+j})\cos^2\left(j\frac{\pi}{180}\right)}{\sum_{j=-45}^{45}\cos\left(j\frac{\pi}{180}\right)}$$

where $F(\varphi_i)$ is the length of the fetch associated with the ith wind direction.

The use of the Breugem and Holthuijsen (2007) formulation is still based on the field data employed by Young and Verhagen (1996), coming from a single study site, Lake George, Australia, even if some site-specific effects have been accounted for. Furthermore, the formulation has been employed successfully by several authors (Carniello et al., 2011; Leonardi et al., 2016b; Mariotti & Fagherazzi, 2013; Tommasini et al., 2019).

Measured sea levels were provided by the Burano gauge of Centro Previsioni e Segnalazioni Maree of Venice Municipality (CPSM; https://www.comune.venezia.it/it/content/centro-previsioni-e-segnalazioni-maree). Since the Burano gauge is located about 2 km north of the monitored marsh, we assumed a quasi-steady propagation of the tidal wave (Toffolon & Lanzoni, 2010) and a negligible wind setup difference. The hypothesis has been verified by reproducing tide propagation and wind setup by means of a two-dimensional coupled hydrodynamic and wind-wave model, which solves the depth-averaged shallow water equations, using a semi-implicit staggered finite element method based on Galerkin's approach (WWTM; Carniello et al., 2005, 2012; Defina, 2000). The equations are suitably modified to account for the wetting and drying processes that occur in shallow and irregular tidal domains (see Defina, 2000; and D'Alpaos & Defina, 2006 for a detailed description of the governing equations and of the numerical scheme).

The wave climate from the Young and Verhagen equations is computed by averaging the wind data collected at Laguna Nord and San Giorgio monitoring stations (CPSM, see Figure 1a), as the marsh we studied is located between these two gauges along the direction of the prevailing winds, which blow with a speed that can easily exceed 10 m/s from the northeastern direction, almost perpendicular to the scarp (Figure 1b). In-field wave climate was measured during 26 storm surges by using two submersible capacitive pressure

transducers, installed and wired in front of the bank scarp, employing the same instrumentation setup and methodology described in Bendoni et al. (2016). The duration of measured storm surges varied from 1 to 7 days. The resolution of the instrument is 0.1 mbar, corresponding to approximately 1 mm of pressure head, with a range of 0.0–100.0 mbar (0.0–1.02 m of pressure head). The sampling rate was set to 6 Hz and the conversion of pressure measurements into wave height is obtained by applying a transfer function on the pressure head measurements based on linear wave theory (Bishop & Donelan, 1987). Data were managed and stored by means of a datalogger (Figure 2c). The measurement of wave climate close to the bank edge during the 26 storm surges allowed us to determine a functional relation between wave height and wave period, measured and computed through the Young and Verhagen model.

The instantaneous value of the wave power projected along the orthogonal direction with respect to the marsh face is then averaged over the considered time span to get the mean wave power [W/m] (see Appendix A). The mean erosion rate [m^2/yr] is determined by multiplying the bank elevation by the average erosion length measured on each pin, dividing it by the considered time interval. The analysis is carried out on the above-mentioned average quantities; hereinafter we refer to them as wave power and erosion rate. The wave power is multiplied by a cosine function depending on the value of the angle that the waves form with the orientation of the marsh face, as proposed by Marani et al. (2011) and confirmed by a sensitivity analysis performed on different functions (see Appendix B). For single surge surveys, both wave power and erosion rate have been computed at four different elevations (i.e. assuming a vertical domain of 0.2 m for each elevation; see Appendix A for more details).

Figure 3 shows the wave climate directional statistics in front of the bank (Figure 3a significant wave height, Figure 3b peak wave period).

3 | RESULTS

3.1 | Data analysis

The retreat of the marsh with respect to a vertical section of the bank was determined by measuring the extent of the erosion on the pin between two subsequent surveys. The time span during which we assumed erosion was determined by summation of the time interval during which wind direction and sea level allowed the waves to hit the bank. Figure 4a illustrates the timeline of the marsh retreat within the surveyed period, accounting for the number of pins used in each monthly survey and the time span between two subsequent monthly surveys. The pin number is not constant, as in monthly surveys some of them were lost and subsequently replaced (Figure 4a, grey line). Figure 4b summarizes the variability in the erosion rate measured by the pins of the single surveys, showing a linear relationship between the average lateral retreat and its standard error, which is about 15% in all three transects. Hereinafter, we refer to measures accounting/not accounting for mass failures (i.e. including/not including the bank retreat due to the collapsed blocks).

The hypothesis of negligible sea level difference between Burano and the surveyed marsh has been confirmed (Figure 5). Concerning the effect of tidal propagation, we found a sea level difference lower than 0.05 m in the period 21–24 December 2019, when a sharp seiche wave enhanced the tidal amplitude up to about 1.3 m (Figure 5a; a rare event for the Burano gauge). Nevertheless, the maximum sea level difference is reached at the crest and at the trough of the tidal wave, when the marsh is either completely submerged, or the low-water level does not even affect the lowest portion of the scarp. Additional wind setup effects can produce a further difference lower than 0.04 cm for wind speeds of 20 m/s, for any wind direction, and lower than 0.02 cm for wind speeds of 16 m/s (Figure 5b), which corresponds to an event with a return period of almost 1 year for northeastern winds in the northern lagoon (Mel & D'Alpaos, 2017).

The measurement of wave climate close to the bank edge during the 26 storm surges supported the calibration of the output from the Young and Verhagen model. Figure 6 compares the significant wave height (a) and wave period (b) measured and estimated by the Young and Verhagen model. Linear regression among data provides

$$H_{measured} = 0.85 \cdot H_{model} \quad (1)$$

$$T_{measured} = 0.80 \cdot T_{model} \quad (2)$$

Furthermore, measured data can overcome the possible shortcomings of the meteo-marine gauges, as occurred in the example reported in Figure C.1, where faulty wind data gauged at San Giorgio station led to underestimating the wave climate (i.e. red dots in Figure 6a).

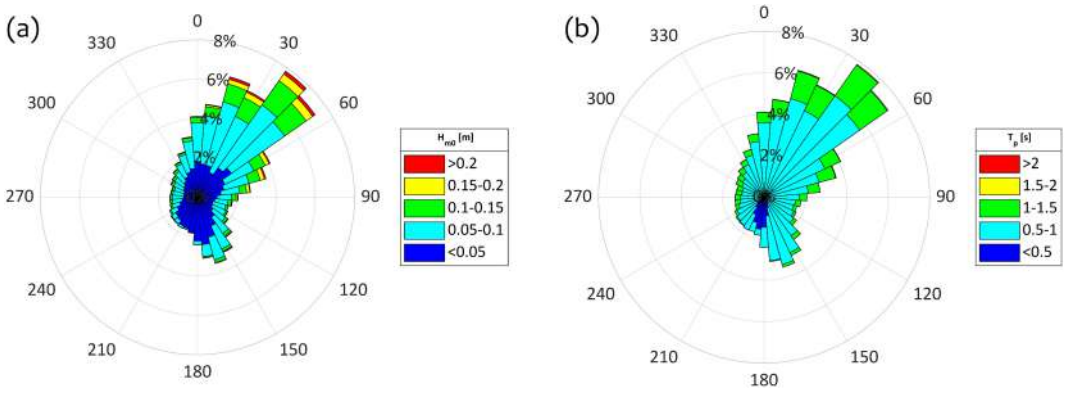

FIGURE 3 Wave rose diagram for 36 cardinal directions computed in front of the monitored marsh. Data have been corrected through Equations (1) and (2). (a) Significant wave height. (b) Peak wave period [Color figure can be viewed at wileyonlinelibrary.com]

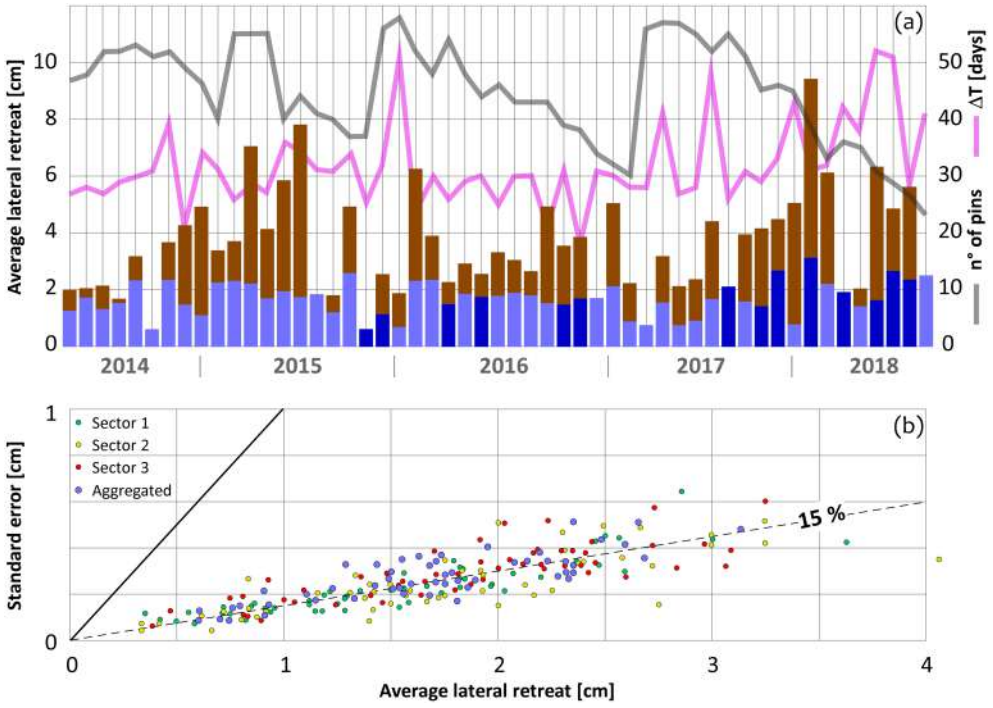

FIGURE 4 (a) Timeline of the performed surveys. Vertical bars illustrate the total lateral retreat measured in each survey. Data are averaged between the three transects. Blue bars account for the retreat not accounting for mass failures; brown bars show the contribution of mass failures. Dark blue bars identify the periods when the surveys at a single meteorological event have been performed in transect 2. Grey line shows the total number of pins deployed in each monthly survey; purple line the time interval elapsed between two consecutive monthly surveys. (b) Relationship between the average lateral retreat and its standard error computed on the basis of the single pin measurements. Black line represents the 1:1 slope [Color figure can be viewed at wileyonlinelibrary.com]

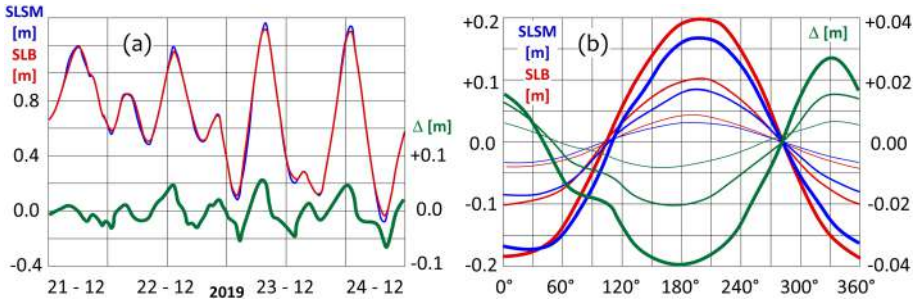

FIGURE 5 Sea level difference (green lines) between Burano gauge (SLB, red lines) and the monitored salt marsh (SLSM, blue lines). (a) Sea level difference due to the tide propagation during a rare event characterized by a tide amplitude greater than 1.2 m. (b) Wind setup for different wind speeds (thick lines 20 m/s, medium lines 16 m/s, thin lines 12 m/s) and for any wind direction [Color figure can be viewed at wileyonlinelibrary.com]

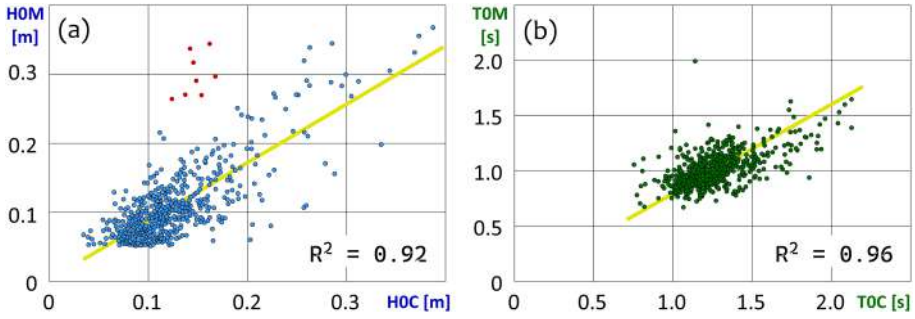

FIGURE 6 Relationship between wave climate measured (H0M, T0M) and computed by the Young and Verhagen model (H0C, T0C). Data where the measured wave height is lower than 0.05 m have not accounted for. (a) Significant wave height. Red dots highlight the erroneous wave climate data collected on 21 November 2015 (see Figure C.1 for the specific analysis of the event). (b) Wave periods [Color figure can be viewed at wileyonlinelibrary.com]

3.2 | Monthly and yearly monitoring campaigns

The monthly and yearly monitoring campaigns confirmed that wave power correlates with erosion rate (Figure 7) through a linear relationship, as theoretically established by Marani et al. (2011) and further verified by empirical analysis based on several observations at different salt marshes worldwide (Leonardi et al., 2016a, b; Priestas et al., 2015) and in the lagoon of Venice (Bendoni et al., 2016; Finotello et al., 2020; Tommasini et al., 2019).

Figure 7a illustrates the relationship between wave power and erosion rate by aggregating the three transects:

i. at monthly time scale (green dots = transect 1, yellow dots = transect 2, red dots = transect 3, grey line = linear regression);
ii. at yearly time scale (blue dots);
iii. at 'annual binned' time scale, hereinafter named binned (i.e. five fictitious bins computed through an equal frequency binning; purple dots).

The same analysis, but not accounting for mass failures, is illustrated in Figure 7b.

Monthly and yearly correlations show good statistical parameters and very similar slopes (Table 1). When mass failures are not accounted for, the regression slope is halved.

Binned data confirm the linear relationship, showing similar R^2 coefficients with respect to the yearly data, but covering a wider spectrum of wave power. In both the analyses reported in Figure 7, binned data denote a slightly lower erosion rate at high wave power than expected from the linear relationship (see the rightmost purple dot), due to some monthly observations characterized by high wave power and modest erosion rate. We argue that in this situation, extremely common in field surveys, these 'outliers' must be included in the statistical analysis. In general, these observations are produced by actual physical processes affecting the marsh, being the most interesting data, if their nature is properly investigated.

Thus, we performed a separate linear regression for each transect to (i) confirm the accuracy of the correlation and (ii) identify the cause of the outliers (Figure 8, Table 2). For all the transects, monthly surveys confirm a stronger correlation if mass failures are not accounted for. Regression slopes are similar, albeit showing different statistical parameters; few outliers (indicated as o_1 to o_9 in Figure 8) are present in all the transects.

If mass failures are accounted for, transects 2 and 3 show a weaker correlation with respect to transect 1, due to a higher ratio (up to 50%) of erosion due to slumping blocks (Table 3). However, in transect 2, mass failures are more occasional, producing, in turn, a slightly lower correlation with respect to transect 3, where mass slumping occurred almost once a month (Table 3). If mass failures are not accounted for, transects 1 and 2 show a robust correlation, whereas in transect 3 data points are more scattered. A possible explanation can be ascribed to the presence of a significant number of blocks collapsed just in front of transect 3, which reduce the actual wave power. Beside the physical processes, we notice significant differences in the lateral retreat mechanism among the three transects (i.e. at a small spatial scale).

Some erosion rate data significantly differ from the linear regression (i.e. a difference greater than three times the root mean square of the absolute differences). For some, we identified the physical processes behind them.

o_1: in this monthly observation, lateral erosion occurs mostly through slumping blocks (i.e. two-thirds of the total retreat), providing an underestimation of the erosion rate if mass failures are not accounted for (Figure 8b), but the point fits the regression line in case of inclusion of the slumping blocks in the statistic (Figure 8a).

o_2–o_6: these represent five subsequent monthly surveys, each one characterized by a different value of wave power (Figures 8c and d). Although the erosion rate correlates well with wave power if mass failures are not accounted for (Figure 8d), we noticed an asynchrony of the slumping blocks, producing a weak correlation if mass failures are accounted for (Figure 8c). However, by averaging the five data points we obtained a wave power of 6.3 W/m and an erosion rate of 1.0 m^2/yr, which is in good agreement with the linear regression, if mass failures are accounted for. This dataset represents an erosion cycle of 5 months, which cannot be described effectively at shorter time scales.

o_7, o_8: these represent another erosion cycle (Figures 8e and f), possibly explained with the highest wave energy flux ever recorded during the 5 years, both when considering a single month (o_7) or the two months (o_7 plus o_8). At the monthly survey between the two periods (o_7 and o_8), we observed that several cantilever profiles promoted by the storms occurred during the period o_7,

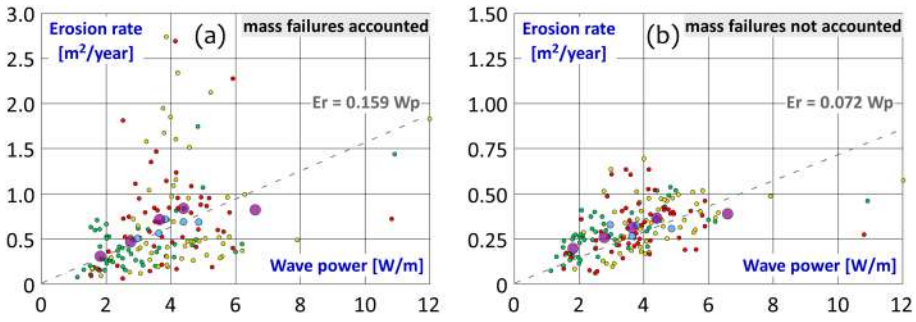

FIGURE 7 Relationship between volumetric erosion rate (E_r) and mean wave power density (W_p). Data are aggregated over the three transects. Small dots illustrate the raw monthly data (green dots, transect 1; yellow dots, transect 2; red dots, transect 3); yearly data (blue dots) and binned data (purple dots). In panel (b) mass failures are not accounted for. Linear regression (grey line) has been computed on the monthly data [Color figure can be viewed at wileyonlinelibrary.com]

TABLE 1 Linear regression of monthly, annual, and binned data computed within the period 2014–2018. Statistical parameters are computed by aggregating the three transects. Grey-shaded cells denote the analysis performed when mass failures are not accounted for

Type of analysis	Slope	R^2	p-Value [5%]	RMSE data [m^2/yr]	RMSE slope [%]
Monthly	0.159	0.66	2.6×10^{-38}	0.502	5.8
Yearly	0.159	0.99	4.5×10^{-4}	0.083	5.9
Binned	0.156	0.95	2.9×10^{-3}	0.161	11.1
Monthly	0.072	0.82	3.9×10^{-61}	0.146	3.7
Yearly	0.079	0.97	1.5×10^{-3}	0.063	8.9
Binned	0.073	0.96	2.4×10^{-3}	0.071	10.4

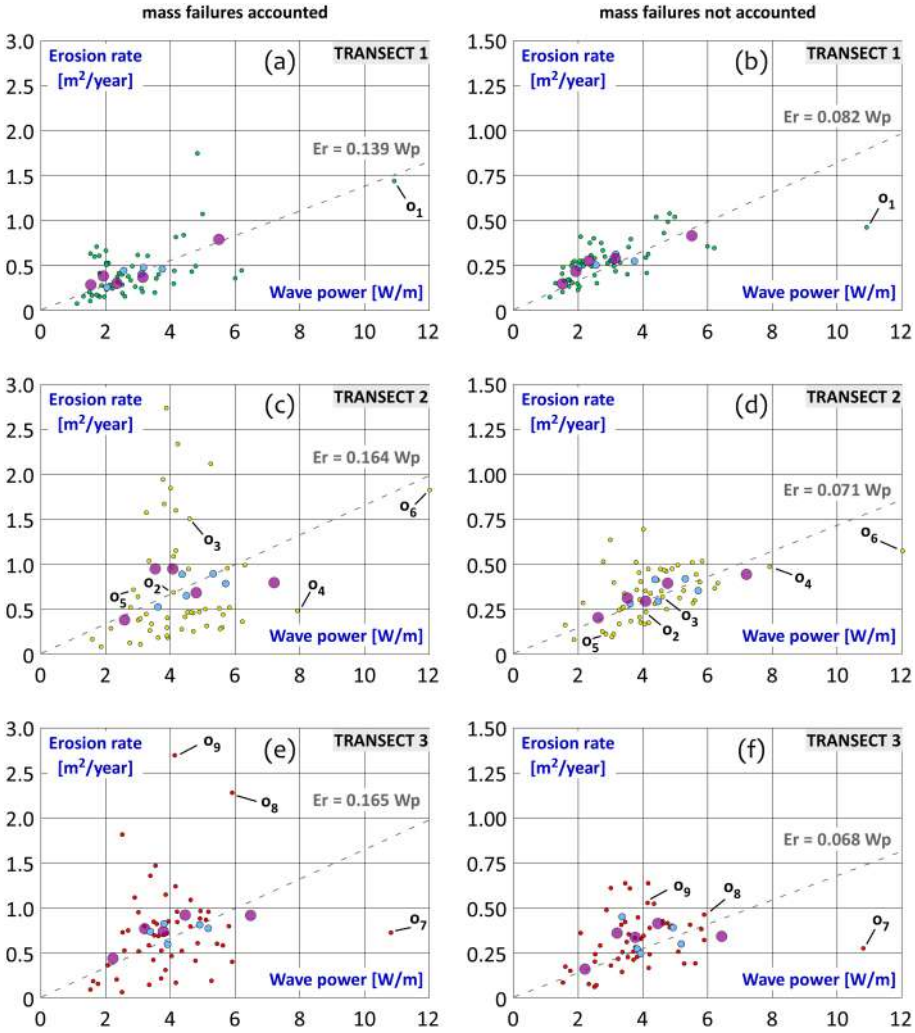

FIGURE 8 Relationship between volumetric erosion rate (E_r) and mean wave power density (W_p) specific to the three transects. Mass failures are not accounted for in right-side panels (b), (d), and (f). Small dots represent the raw monthly data, to which the regression line refers; blue dots the yearly data and purple dots the binned data. o_1–o_9 represent the 'outliers' we investigated [Color figure can be viewed at wileyonlinelibrary.com]

TABLE 2 Linear regression of the monthly data computed within the period 2014–2018. Statistical parameters are computed for each transect and by aggregating the data. In grey-shaded rows, mass failures are not accounted for

ID transect	Slope	R^2	*p*-Value [5%]	RMSE data [m²/yr]	RMSE slope [%]
1	0.139	0.77	5.0×10^{-18}	0.256	7.6
2	0.164	0.62	1.6×10^{-12}	0.641	10.8
3	0.165	0.67	6.4×10^{-14}	0.533	9.8
AGG	0.159	0.66	2.6×10^{-38}	0.502	5.8
1	0.082	0.86	1.5×10^{-23}	0.112	5.6
2	0.071	0.86	8.0×10^{-24}	0.142	5.5
3	0.068	0.76	9.1×10^{-18}	0.173	7.7
AGG	0.072	0.82	3.9×10^{-61}	0.146	3.7

TABLE 3 Dataset 2014–2018. Fraction of erosion due to mass failures, frequency of occurrence of one or more mass failures between two consecutive monthly surveys; R^2 with and without accounting for mass failures in monthly and yearly analysis

ID transect	MF erosion [%]	MF occurrence [%]	R^2 MF monthly	R^2 MF yearly	R^2 no MF monthly	R^2 no MF yearly
1	36.2	39.6	0.77	0.98	0.86	0.98
2	55.4	41.5	0.62	0.98	0.86	0.98
3	57.6	77.4	0.67	0.97	0.76	0.91

resulting in mass failures during the subsequent month (o_8), when the wave power was still significant to trigger the slumping of the blocks.

o_9: this shows an exceptional erosion produced by nine mass failures occurring between two monthly surveys. The collapse of the blocks occurred at the beginning of the spring of the year 2015, after

four winter months characterized by moderate wave power (4 W/m) and low erosion rates (almost 0.6 m^2/yr, accounting for mass failures).

3.3 | Storm surge monitoring campaigns

To investigate the retreat mechanism at a short time scale, we studied 26 storms that occurred in the period 2015–2018, characterized by wind blowing from several directions with a speed range from 1 to 20 m/s. These storms triggered wave heights covering the range 0.05–0.5 m at different water levels in front of the bank. In addition, no mass failures or cantilever profiles were observed during the surveys that followed the storms. We compared the ratio between volumetric erosion rate and wave energy flux among seven groups of pins located at four different elevations with respect to the bank toe (Figure 9b).

Figure 9a confirms the linear relationship between wave power and erosion rate ($R^2 = 0.73$, RMSE of the slope < 10%), showing a similar slope as that computed from the monthly and yearly surveys on transect 2 (Figure 8d). Figure 9b compares the regression lines computed separately for each elevation of the pins [i.e. from −0.15 m to +0.15 m above sea level (a.s.l.)]. The most important result consists in the higher slope of the regression at lower elevations (Figure 10), specifically elevations 1 and 2, where we noticed an almost double erosion rate, despite a lower wave power impinging on the portion of the bank located below mean sea level. Since all transects (1–3) show cantilever failures, which produce almost half of the lateral retreat (Figure 4a), we argue that the results of Figure 9b are not an isolated, rare case. In general, cantilever failures (i.e. higher erosion at the lower portion of the bank) can be produced by two different processes: (a) a higher wave power impinging on the lower part of the scarp; (b) a higher ratio between erosion rate and wave power (i.e. the slope of the regression). To confirm that, in the surveyed marsh, process (b) governs the erosion mechanism, we computed for the entire surveyed period (2014–2018) the cumulative wave power in front of the marsh at eight elevations (from −0.35 to +0.35 m a.s.l.; see Figure 10). The results show a positive correlation between wave power and bank elevation for all three transects. As the surveyed marsh shows cantilever profiles, our outcomes show that, at lower elevations, a lower wave power must result in a higher slope of the correlation between erosion rate and wave power, confirming the findings at short time scale reported in Figure 9b.

4 | DISCUSSION

On a monthly time scale, we noticed a stronger correlation between wave power and erosion rate if no mass failures are accounted for (Figure 7, Table 1). This can be explained by the possible asynchronism at the time scale of a single month between the slumping of the blocks and the wave forcing inducing the mass failures. In general, months characterized by high wave energy can prepare bank morphology for a mass failure, which can occur later and not necessarily be related to a significant wave energy flux. On a yearly time scale, this phenomenon is less relevant, indeed slumped blocks are in general not completely removed after several weeks or months, providing an additional defence for the bank. This agrees with the previous finding by Tommasini et al. (2019). Thus, on a yearly time scale, we noticed a stronger correlation even if mass failures are accounted for, highlighting the importance of selecting the proper time scale based on the type of analysis.

Figure 8 shows that lateral erosion promoted by mass failures can occur over cycles of multiple months, producing a possible weaker fit of the single observation with the regression line, particularly if mass failures are accounted for. However, the slumping of blocks may also occur randomly, since the presence and duration of the erosion cycle depend on multiple physical processes and on the local morphology of the scarp, which can vary within the same transect in a small area. Furthermore, we observed that mass failures may be triggered by one or more single strong storms, and that possible inaccuracy in wind-wave climate estimation in front of the bank, if not gauged *in situ* (Figures. 5a and C.1b), can affect the proper identification of the erosion cycles. We stress that mass failure prediction is particularly problematic when wave energy fluxes reaching the marsh edge are relatively low as in the surveyed area, as pointed out by Bendoni et al. (2016) and Leonardi et al. (2016b), particularly affecting the analysis performed on monthly time scales (Table 3).

On a single storm time scale (Figure 9), the lower slope of the regression for the upper portion of the bank might be due to interplay between soil characteristics and the presence of a root mat, which increases the resistance of the upper part of the bank to the erosion process. Furthermore, when waves impact the scarp toe, they generally break with high turbulence, negligible wave reflection, and a significant wave runup, enhancing the erosion at low tide. This is a possible, robust explanation of the presence of the cantilever profiles in this marsh, as also found by Bendoni et al. (2016). In other intertidal

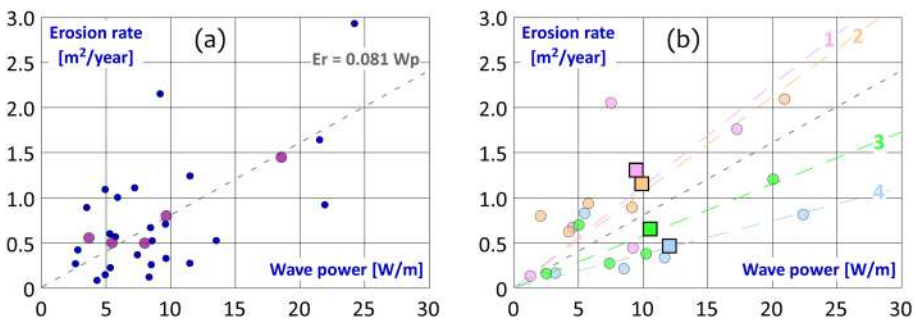

FIGURE 9 Relationship between volumetric erosion rate (E_r) and mean wave power (W_p) computed on a single surge time scale through the measured wave climate. (a) Aggregate data of each event; purple dots represent the binned data. (b) Binned data for each elevation of the pins. The squares aggregate all the storms for a specific elevation (elevation 1, −0.15 m a.s.l., pink; elevation 2, −0.05 m a.s.l., orange; elevation 3, +0.05 m a.s.l., green; elevation 4, +0.15 m a.s.l., blue) [Color figure can be viewed at wileyonlinelibrary.com]

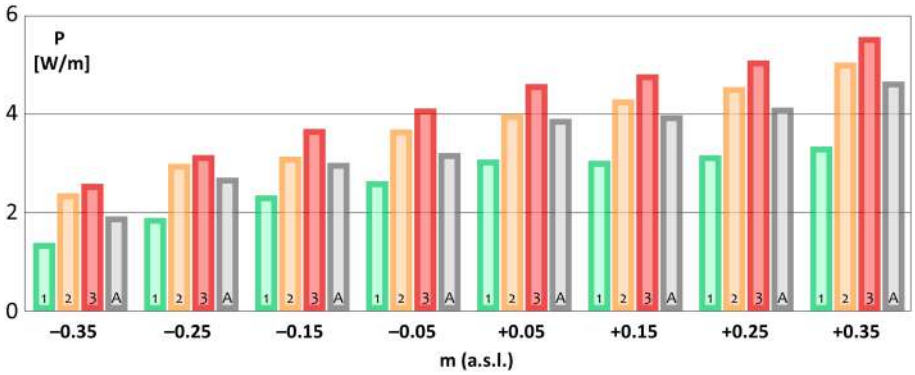

FIGURE 10 Relationship between the elevation of the scarp and wave power computed on the 2014–2018 data: transect 1 (green), 2 (orange), 3 (red), aggregated data (grey) [Color figure can be viewed at wileyonlinelibrary.com]

areas, wave power could be much greater at the marsh top (e.g. if the fetch is much larger when sea level increases), producing a higher erosion at the top despite its greater resistance to wave attack.

The regression slope we found at all time scales (Figures 7–9) falls within the range of variability typically observed for salt marshes in the Venice Lagoon (Marani et al., 2011; Tommasini et al., 2019; Finotello et al., 2020). Large slopes are due to the use of wind data measured at the lagoonal gauges to force the wave model, which show values significantly lower (up to 50%) with respect to the seaward gauges used in other studies (e.g. Diga Sud Chioggia, located about 2 km in front of the southern margin of the Venice Lagoon as in Finotello et al., 2020; Tommasini et al., 2019). We argue that the use of Diga Sud Chioggia is not representative of the wind climate of the northern Venice Lagoon, not only providing an overestimation of the wind speed compared to Laguna Nord gauge (15–20% on average, see Appendix C), but also showing significant data scattering (Table C.3). We also observed different wind directions between two lagoonal CPSM wind gauges, reducing the accuracy of a reliable estimation of the wave climate. Furthermore, the implementation of the wave model based on field data produced an additional reduction of the wave power directly computed from Laguna Nord and San Giorgio gauges by a factor ≅0.6 (Figure 6).

Our findings support recent studies which claimed that wind climate governs the erosion process in the marshes only at large spatial and temporal scales, while different external (e.g. foreshore wave climate, water level in front of the scarp) and internal (e.g. morphology of the marsh, soil and vegetation properties and their role in preventing salt marsh erosion) factors control the retreat of salt marsh edges at smaller scales (Feagin et al., 2009; Wang et al., 2017).

The relationship between water depth and the effectiveness of wave power in producing erosion (Figure 10) stimulates the analysis and quantification of how RSLR could affect lateral retreat. Mel et al. (2019) report RSLR of about 6 mm/yr over the last 30 years in the Venice Lagoon; IPCC scenarios (IPCC, 2013) indicate that sea level rise is likely to intensify the flooding frequency in the next few decades (without accounting for the possible effects of local subsidence); Bondesan et al. (1995) and Mel et al. (2013) show that the increasing sea level would not affect tidal amplitude, surge heights, and wind climate. Possible future scenarios for the salt marshes of the Venice Lagoon driven by climate change depend also on many other factors, such as the morphologic evolution of the tidal flat in front of the bank and the rate of vertical accretion, therefore we encourage further investigations to enlighten the effect of RSLR on marsh lateral retreat. Furthermore, it will be crucial to understand the effect of the operation of the Mo.S.E. barriers on sea level and sediment transport (Mel, 2021; Tognin et al., 2021; Mel et al., 2021a,b).

All the aspects highlighted here are of paramount importance for conservation and restoration, allowing stakeholders to assign specific morphology and vegetation cover to restore marshes, based on the morphodynamic and ecological functions they must fulfil (Finotello et al., 2020), and in relation to an effective ecosystem-based coastal protection (Day et al., 2007; Temmerman et al., 2013). However, this analysis considers only lateral retreat, therefore many other processes could affect the evolution of a specific marsh (e.g. the drowning of the marshes that would lead to irreversible marsh loss; see Mariotti, 2020).

5 | CONCLUSIONS

A 5-year monitoring campaign has been carried out in a salt marsh located in the northern Venice Lagoon. Wave forcing has been determined through both *in-situ* field measurements and mathematical modelling based on wind climate, fetch, sea level, and bathymetry. The target here is to highlight the relationship between wind waves and lateral retreat of salt marsh margins at different time scales and to report the most common issues faced in the monitoring campaigns.

Specifically, the five questions reported in the abstract have been addressed. (i) *What is the relationship between wave climate and erosion rate at different time scales?* On a yearly, monthly, and single storm time scale we derived the same slope of the regression line between wave power and erosion rate. If mass failures are not accounted for, the slope of the regression almost halved. Results are valid if we analyse the three transects separately. Furthermore, on a monthly time scale, we found a better correlation if cantilever failures are not included in the analysis, since the relationship between wave energy flux and slumping blocks occurs over several months, due to the crucial role played by internal and external factors that govern the timing and amount of mass failures. Although an unstable cantilever configuration of the bank is triggered by intense wave attacks, the collapse of unstable blocks is not necessarily correlated with the instantaneous wave forcing. However, months characterized by higher wave forcing show a more frequent occurrence of mass failure events. (ii) *How can the surveys based on a single meteorological event support large-scale monitoring campaigns?* Through a monitoring campaign on a single storm surge time scale, we demonstrated that the slope of the regression line between wave power and erosion rate is higher at the lowest portion of the bank, which is less resistant to wave attack. This

behaviour explains the presence of cantilever profiles in the monitored area. (iii) *What are the main meteorological and morphological parameters correlated to the erosion process?* The main factors are wave climate and hydrodynamic level, together with the elevation and vegetation of the marsh. In this study, we noticed significant retreat differences in different transects within the same marsh. This result highlights the importance of local factors promoting the erosion process. (iv) *Why do only some marshes show cantilever profiles?* In some intertidal areas, waves break before impacting the scarp toe, producing high runup and turbulence, and negligible wave reflection. In other areas, wave power could be much greater at the marsh top, producing a higher erosion at the top despite its greater resistance to wave attack. Furthermore, the presence of vegetation can play a fundamental role in the soil strength of the top of the scarp, indicating a potential to delay the marsh edge erosion. The result is consistent with early claims that a root mat effectively acts to limit marsh erosion, suggesting that the planting and conservation of edge-stabilizing species on salt marshes are key restoration projects. (v) *What are the most common issues to deal with in monitoring campaigns?* We show that wind climate varies even at short distances, and it is crucial to validate the wave models with field measurements. However, faulty wind-wave data are often masked by large time and spatial scale analysis, particularly if the marsh bank is affected by a predominant wind direction. Thus, selecting the location of the marsh on the basis of the existing monitoring network is crucial to obtain a robust wind and tide dataset. Furthermore, a weak correlation between wave power and erosion rate can be noticed if the process is characterized by a random slumping of blocks. Mass failures can occur over long-period cycles, which are related to multiple physical processes and to the local morphology of the scarp and, in turn, may vary almost randomly in time and space.

The linear relationship between wave power and erosion rate, recurring at all time scales, reinforces earlier proposals to use such a relationship as a valuable tool for long-term morphodynamical analyses. However, many open issues still remain to be analysed; for example, the duration of the cantilever failure cycles and the long-term influence of RSLR. Even though more analyses are required to better understand the effect of the single processes involved in lateral retreat of salt marsh margins, our monitoring campaign might provide valuable guidelines to better design effective and reliable salt marsh field measurements.

ACKNOWLEDGEMENTS

We acknowledge the University of Florence for the datalogger, drowned in the exceptional flood that affected Venice on 12 November 2019; Professors Luca Solari and Stefano Lanzoni for fruitful discussions; and Dr Enrica Belluco for offering help and resources to perform the campaign. Open Access Funding provided by Universita della Calabria within the CRUI-CARE Agreement. [Correction added on 20 May 2022, after first online publication: CRUI funding statement has been added.]

FUNDING

This research did not receive any specific grant from funding agencies in the public, commercial, or not-for-profit sectors.

AUTHOR CONTRIBUTIONS

RAM: conceptualization, methodology, investigation, data curation, validation, visualization, writing – original draft, writing – review and editing. **MB**: conceptualization, methodology, data curation, validation, visualization, writing – review and editing. **DS**: methodology, investigation, data curation, validation, visualization.

DATA AVAILABILITY STATEMENT

Data are available on request from the authors.

ORCID

Riccardo A. Mel https://orcid.org/0000-0002-5534-7170

REFERENCES

Barbier, E.B., Hacker, S.D., Kennedy, C., Koch, E.W., Stier, A.C. & Silliman, B.R. (2011) The value of estuarine and coastal ecosystem services. *Ecological Monographs*, 81(2), 169–193. Available from: https://doi.org/10.1890/10-1510.1

Bendoni, M., Georgiou, I.Y., Roelvink, D. & Oumeraci, H. (2019) Numerical modelling of the erosion of marsh boundaries due to wave impact. *Coastal Engineering*, 152, 103514. Available from: https://doi.org/10.1016/j.coastaleng.2019.103514

Bendoni, M., Mel, R., Lanzoni, S., Francalanci, S., Oumeraci, H. & Solari, L. (2016) Insights into lateral marsh retreat mechanism through localized field measurements. *Water Resources Research*, 52(2), 1446–1464. Available from: https://doi.org/10.1002/2015WR017966

Bishop, C.T. & Donelan, M.A. (1987) Measuring waves with pressure transducers. *Coastal Engineering*, 11(4), 309–328. Available from: https://doi.org/10.1016/0378-3839(87)90031-7

Boicourt, W.C. (1993) Estuaries: Where the river meets the sea. *Oceanus*, 36(2), 29–37.

Bondesan, M., Castiglioni, G., Elmi, C., Gabbianelli, G., Marocco, R., Pirazzoli, P.A. & Tomasin, A. (1995) Coastal areas at risk from storm surges and sea-level rise in northeastern Italy. *Journal of Coastal Research*, 11(4), 1354–1379.

Bouma, T.J., van Belzen, J., Balke, T., Zhu, Z., Airoldi, L., Blight, A.J., Davies, A.J., Galvan, C., Hawkins, S.J. & Hoggart, S.P. (2014) Identifying knowledge gaps hampering application of intertidal habitats in coastal protection: Opportunities & steps to take. *Coastal Engineering*, 87, 147–157. Available from: https://doi.org/10.1016/j.coastaleng.2013.11.014

Breugem, W.A. & Holthuijsen, L.H. (2007) Generalized shallow water wave growth from Lake George. *Journal of Waterway Port, Coastal, and Ocean Engineering*, 133(3), 173–182. Available from: https://doi.org/10.1061/(ASCE)0733-950X(2007)133:3(173)

Carniello, L., D'Alpaos, A. & Defina, A. (2011) Modeling wind waves and tidal flows in shallow micro-tidal basins. *Estuarine, Coastal and Shelf Science*, 92(2), 263–276. Available from: https://doi.org/10.1016/j.ecss.2011.01.001

Carniello, L., Defina, A. & D'Alpaos, L. (2009) Morphological evolution of the Venice Lagoon: Evidence from the past and trend for the future. *Journal of Geophysical Research – Earth Surface*, 114(F4), 1–10. Available from: https://doi.org/10.1029/2008JF001157

Carniello, L., Defina, A. & D'Alpaos, L. (2012) Modeling sand–mud transport induced by tidal currents and wind waves in shallow microtidal basins: Application to the Venice Lagoon (Italy). *Estuarine, Coastal and Shelf Science*, 102–103, 105–115. Available from: https://doi.org/10.1016/j.ecss.2012.03.016

Carniello, L., Defina, A., Fagherazzi, S. & D'Alpaos, L. (2005) A combined wind wave-tidal model for the Venice Lagoon, Italy. *Journal of Geophysical Research - Earth Surface*, 110(F4), F04007. Available from: https://doi.org/10.1029/2004JF000232

Cosma, M., Ghinassi, M., D'Alpaos, A., Roner, M., Finotello, A., Tommasini, L. & Gatto, R. (2019) Point-bar brink and channel thalweg trajectories depicting interaction between vertical and lateral shifts of microtidal channels in the Venice Lagoon (Italy). *Geomorphology*, 342, 37–50. Available from: https://doi.org/10.1016/j.geomorph.2019.06.009

Costanza, R., Déarge, R., de Groot, R., Farber, S., Grasso, M., Hannon, B., Limburg, K.E. & Naeem, S. (1997) The value of the world's ecosystem services and natural capital. *Nature*, 387(6630), 253–260. Available from: https://doi.org/10.1038/387253a0

Craft, C., Clough, J., Ehman, J., Joye, S., Park, R., Pennings, S., Guo, H. & Machmuller, M. (2008) Forecasting the effects of accelerated sea-level rise on tidal marsh ecosystem services. *Frontiers in Ecology and the Environment*, 7(2), 73–78.

D'Alpaos, A., Carniello, L. & Rinaldo, A. (2013) Statistical mechanics of wind wave-induced erosion in shallow tidal basins: Inferences from the Venice Lagoon. *Geophysical Research Letters*, 40(13), 3402–3407. Available from: https://doi.org/10.1002/grl.50666

D'Alpaos, A., Mudd, S.M. & Carniello, L. (2011) Dynamic response of marshes to perturbations in suspended sediment concentrations and rates of relative sea level rise. *Journal of Geophysical Research – Earth Surface*, 116(F4), 1–13. Available from: https://doi.org/10.1029/2011JF002093

D'Alpaos, L. & Defina, A. (2006) Mathematical modeling of tidal hydrodynamics in shallow lagoons: A review of open issues and applications to the Venice Lagoon. *Computers and Geosciences*, 33(4), 476–496. Available from: https://doi.org/10.1016/j.cageo.2006.07.009

D'Alpaos, L. & Martini, P. (2005) The influence of inlet configuration on sediment loss in the Venice Lagoon. In: Fletcher, C.A. & Spencer, T. (Eds.) *Flooding and Environmental Challenges for Venice and its Lagoon: State of Knowledge*. Cambridge: Cambridge University Press, pp. 419–430.

Day, J.W., Boesch, D.F., Clairain, E.J., Kemp, G.P., Laska, S.B., Mitsch, W.J., Orth, K., Mashriqui, H., Reed, D.J., Shabman, L., Simenstad, C.A., Streever, B.J., Twilley, R.R., Watson, C.C., Wells, J.T. & Whigham, D. F. (2007) Restoration of the Mississippi Delta: Lessons from hurricanes Katrina and Rita. *Science*, 315(5819), 1679–1684. Available from: https://doi.org/10.1126/science.1137030

Defina, A. (2000) Two-dimensional shallow flow equations for partially dry areas. *Water Resources Research*, 36(11), 3251–3264. Available from: https://doi.org/10.1029/2000WR900167

Deheyn, D.D. & Shaffer, L.R. (2007) Saving Venice: Engineering and ecology in the Venice Lagoon. *Technology in Society*, 29(2007), 205–221. Available from: https://doi.org/10.1016/j.techsoc.2007.01.014

Evans, B., Möller, I. & Spencer, T. (2021) Topological and morphological controls on morphodynamics of salt marsh interiors. *Journal of Marine Science and Engineering*, 9(3), 311. Available from: https://doi.org/10.3390/jmse9030311

Evans, B.R., Möller, I., Spencer, T. & Smith, G. (2019) Dynamics of salt marsh margins are related to their three-dimensional functional form. *Earth Surface Processes and Landforms*, 44(9), 1816–1827. Available from: https://doi.org/10.1002/esp.4614

Fagherazzi, S., Mariotti, G., Leonardi, N., Canestrelli, A., Nardin, W. & Kearney, W.S. (2020) Salt marsh dynamics in a period of accelerated sea level rise. *Journal of Geophysical Research – Earth Surface*, 125(8), e2019JF005200. Available from: https://doi.org/10.1029/2019JF005200

Fagherazzi, S., Mariotti, G., Wiberg, P.L. & McGlathery, K.J. (2013) Marsh collapse does not require sea level rise. *Oceanography*, 26(3), 70–77. Available from: https://doi.org/10.5670/oceanog.2013.47

Falcão, M., Santos, M.N., Drago, T., Serpa, D. & Monteiro, C. (2009) Effect of artificial reefs (southern Portugal) on sediment–water transport of nutrients: Importance of the hydrodynamic regime. *Estuarine, Coastal and Shelf Science*, 83(4), 451–459. Available from: https://doi.org/10.1016/j.ecss.2009.04.028

Feagin, R.A., Lozada-Bernard, S.M., Ravens, T.M., Möller, I., Yeager, K.M. & Baird, A.H. (2009) Does vegetation prevent wave erosion of salt marsh edges? *Proceedings of the National Academy of Sciences of the United States of America*, 106(25), 10109–10113. Available from: https://doi.org/10.1073/pnas.0901297106

Findell, K.L., Berg, A., Gentine, P., Krasting, J.P., Lintner, B.R., Malyshev, S., Santanello, J.A. & Shevliakova, E. (2017) The impact of anthropogenic land use and land cover change on regional climate extremes. *Nature Communications*, 8(1), 989. Available from: https://doi.org/10.1038/s41467-017-01038-w

Finotello, A., Lanzoni, S., Ghinassi, M., Marani, M., Rinaldo, A. & D'Alpaos, A. (2018) Field migration rates of tidal meanders recapitulate fluvial morphodynamics. *Proceedings of the National Academy of Sciences*, 115(7), 1463–1468. Available from: https://doi.org/10.1073/pnas.1711330115

Finotello, A., Marani, M., Carniello, L., Pivato, M., Roner, M., Tommasini, L. & D'Alpaos, A. (2020) Control of wind-wave power on morphological shape of salt marsh margins. *Water Science and Engineering*, 13(1), 45–46. Available from: https://doi.org/10.1016/j.wse.2020.03.006

FitzGerald, D.M. & Hughes, Z. (2019) Marsh processes and their response to climate change and sea-level rise. *Annual Review of Earth and Planetary Sciences*, 47(1), 481–517. Available from: https://doi.org/10.1146/annurev-earth-082517-010255

Fourqurean, J.W., Duarte, C.M., Kennedy, H., Marbà, N., Holmer, M., Mateo, M.A., Apostolaki, E.T., Kendrick, G.A., Krause-Jensen, D. & McGlathery, K.J. (2012) Seagrass ecosystems as a globally significant carbon stock. *Nature Geoscience*, 5(7), 505–509. Available from: https://doi.org/10.1038/ngeo1477

Gedan, K.B., Silliman, B.R. & Bertness, M.D. (2009) Centuries of human-driven change in saltmarsh ecosystems. *Annual Review of Marine Science*, 1(1), 117–141. Available from: https://doi.org/10.1146/annurev.marine.010908.163930

Ghinassi, M., Brivio, L., D'Alpaos, A., Finotello, A., Carniello, L., Marani, M. & Cantelli, A. (2018) Morphodynamic evolution and sedimentology of a microtidal meander bend of the Venice Lagoon (Italy). *Marine and Petroleum Geology*, 96, 391–404. Available from: https://doi.org/10.1016/j.marpetgeo.2018.06.011

Howes, N., FitzGerald, D.M., Hughes, Z.J., Georgiou, I.Y., Kulp, M., Miner, M.D., Smith, J.M. & Barras, J. (2010) Hurricane-induced failure of low salinity wetlands. *Proceedings of the National Academy of Sciences of the United States of America*, 107(32), 14014–14019. Available from: https://doi.org/10.1073/pnas.0914582107

IPCC. (2013) Annex II: Climate system scenario tables. In: Prather, M., Flato, G., Friedlingstein, P., Jones, C., Lamarque, J.-F., Liao, H. & Rasch, P. (Eds.) *Climate Change 2013: The Physical Science Basis. Contribution of Working Group I to the Fifth Assessment Report of the Intergovernmental Panel on Climate Change* [Stocker TF, Qin D, Plattner G-K, Tignor M, Allen SK, Boschung J, Nauels A, Xia Y, Bex V, Midgley PM (eds)]. Cambridge: Cambridge University Press.

Leonardi, N., Defne, Z., Ganju, N.K. & Fagherazzi, S. (2016a) Salt marsh erosion rates and boundary features in a shallow bay. *Journal of Geophysical Research – Earth Surface*, 121(10), 1861–1875. Available from: https://doi.org/10.1002/2016JF003975

Leonardi, N., Ganju, N.K. & Fagherazzi, S. (2016b) A linear relationship between wave power and erosion determines salt-marsh resilience to violent storms and hurricanes. *Proceedings of the National Academy of Sciences*, 113(1), 64–68. Available from: https://doi.org/10.1073/pnas.1510095112

Luternauer, J.L., Atkins, R.J., Moody, A.I., Williams, H.E. & Gibson, J.W. (1995) Salt marshes. In: *Developments in Sedimentology*, Vol. 53. Elsevier, pp. 307–332. Available from: https://doi.org/10.1016/S0070-4571(05)80031-7.

Marani, M., D'Alpaos, A., Lanzoni, S. & Santalucia, M. (2011) Understanding and predicting wave erosion of marsh edge. *Geophysical Research Letters*, 38(21), L21401. Available from: https://doi.org/10.1029/2011GL048995

Marani, M., Silvestri, S., Belluco, E., Ursino, N., Comerlati, A., Tosatto, O. & Putti, M. (2006) Spatial organization and ecohydrological interactions in oxygen-limited vegetation ecosystems. *Water Resources Research*, 42(6), W06D06. Available from: https://doi.org/10.1029/2005WR004582

Mariotti, G. (2020) Beyond marsh drowning: The many faces of marsh loss (and gain). *Advances in Water Resources*, 144, 103710. Available from: https://doi.org/10.1016/j.advwatres.2020.103710

Mariotti, G. & Fagherazzi, S. (2013) Critical width of tidal flats triggers marsh collapse in the absence of sea-level rise. *Proceedings of the National Academy of Sciences of the United States of America*, 110(14), 5353–5356. Available from: https://doi.org/10.1073/pnas.1219600110

Mariotti, G., Fagherazzi, S., Wiberg, P.L., McGlathery, K.J., Carniello, L. & Defina, A. (2010) Influence of storm surges and sea level on shallow tidal basin erosive processes. *Journal of Geophysical Research, Oceans*,

115(C11), C11012. Available from: https://doi.org/10.1029/2009JC005892

Mel, R. (2021) Exploring the partial use of the Mo.S.E. system as effective adaptation to rising flood frequency of Venice. *Natural Hazards and Earth System Sciences*, 21(12), 3629–3644. Available from: https://doi.org/10.5194/nhess-21-3629-2021

Mel, R., Carniello, L. & D'Alpaos, L. (2019) Addressing the effect of the Mo.S.E. barriers closure on wind setup within the Venice lagoon. *Estuarine, Coastal and Shelf Science*, 225, 106249. Available from: https://doi.org/10.1016/j.ecss.2019.106249

Mel, R., Carniello, L. & D'Alpaos, L. (2021a) How long will the Mo.S.E. barriers be effective in protecting all urban settlements within the Venice Lagoon? The wind setup constraint. *Coastal Engineering*, 168, 103923. Available from: https://doi.org/10.1016/j.coastaleng.2021.103923

Mel, R., Carniello, L., Viero, D.P., Defina, A. & D'Alpaos, L. (2021b) The first operations of Mo.S.E. system to prevent the flooding of Venice: Insights on the hydrodynamics of a regulated lagoon. *Estuarine, Coastal and Shelf Science*, 261, 107547. Available from: https://doi.org/10.1016/j.ecss.2021.107547

Mel, R. & D'Alpaos, L. (2017) *Un criterio semplificato per il controllo degli allagamenti dei centri storici causati dai sovralzi indotti dal vento durante le fasi di chiusura delle bocche di porto*, *Commissione di studio sui problemi di Venezia*, Vol. III. Venezia: Istituto Veneto di SS.LL.AA.

Mel, R., Sterl, A. & Lionello, P. (2013) High resolution climate projection of storm surge at the Venetian coast. *Natural Hazards and Earth System Sciences*, 13(4), 1135–1142. Available from: https://doi.org/10.5194/nhess-13-1135-2013

Mitsch, W.J. & Gosselink, J.G. (2000) The value of wetlands: Importance of scale and landscape setting. *Ecological Economics*, 35(1), 25–33. Available from: https://doi.org/10.1016/S0921-8009(00)00165-8

Molinaroli, E., Guerzoni, S., Sarretta, A., Masiol, M. & Pistolato, M. (2009) Thirty-year changes (1970 to 2000) in bathymetry and sediment texture recorded in the Lagoon of Venice sub-basins, Italy. *Marine Geology*, 258(1–4), 115–125. Available from: https://doi.org/10.1016/j.margeo.2008.12.001

Möller, I., Kudella, M., Rupprecht, F., Spencer, T., Paul, M., van Wesenbeeck, B.K., Wolters, G., Jensen, K., Bouma, T.J., Lange, M. M. & Schimmels, S. (2014) Wave attenuation over coastal salt marshes under storm surge conditions. *Nature Geoscience*, 7(10), 727–731. Available from: https://doi.org/10.1038/ngeo2251

Moller, L. (1999) Wave transformation over a salt marsh: A field and a numerical modeling study from North Norfolk, England. *Estuarine, Coastal and Shelf Science*, 49(3), 411–426. Available from: https://doi.org/10.1006/ecss.1999.0509

Moller, L. (2006) Quantifying saltmarsh vegetation and its effect on wave height dissipation: Results from a UK east coast saltmarsh. *Estuarine, Coastal and Shelf Science*, 69(3–4), 337–351. Available from: https://doi.org/10.1016/j.ecss.2006.05.003

Priestas, A.M. & Fagherazzi, S. (2011) Morphology and hydrodynamics of wave-cut gullies. *Geomorphology*, 131(1–2), 1–13. Available from: https://doi.org/10.1016/j.geomorph.2011.04.004

Priestas, A.M., Mariotti, G., Leonardi, N. & Fagherazzi, S. (2015) Coupled wave energy and erosion dynamics along a salt marsh boundary, Hog Island Bay, Virginia, USA. *Journal of Marine Science and Engineering*, 3(3), 1041–1065. Available from: https://doi.org/10.3390/jmse3031041

Ratliff, K.M., Braswell, A.E. & Marani, M. (2015) Spatial response of coastal marshes to increased atmospheric CO_2. *Proceedings of the National Academy of Sciences*, 112(51), 15580–15584. Available from: https://doi.org/10.1073/pnas.1516286112

Rogers, K. & Woodroffe, C.D. (2014) Tidal flats and salt marshes. In: Masselink, G. & Gehrels, R. (Eds.) *Coastal Environments and Global Change*. Chichester: Wiley, pp. 227–250.

Sarretta, A., Pillon, S., Molinaroli, E., Guerzoni, S. & Fontolan, G. (2010) Sediment budget in the Lagoon of Venice, Italy. *Continental Shelf Research*, 30(8), 934–949. Available from: https://doi.org/10.1016/j.csr.2009.07.002

Saville T. 1954. *The Effect of Fetch Width on Wave Generation*. Technical Memorandum 70. Beach Erosion Board: Washington, D.C.

Schoutens, K., Heuner, M., Fuchs, E., Minden, V., Schulte-Ostermann, T., Belliard, J.P., Bouma, T.J. & Temmerman, S. (2020) Nature-based shoreline protection by tidal marsh plants depends on trade-offs between avoidance and attenuation of hydrodynamic forces. *Estuarine, Coastal and Shelf Science*, 236, 106645. Available from: https://doi.org/10.1016/j.ecss.2020.106645

Schwimmer, M.M. (2001) Rates and processes of marsh shoreline in Rehoboth Bay, Delaware, USA. *Journal of Coastal Research*, 17(3), 672–683.

Silvestri, S. & Marani, M. (2004) Salt-marsh vegetation and morphology: Basic physiology, modelling and remote sensing observations. In: Fagherazzi, S., Marani, M. & Blum, L. (Eds.) *The Ecogeomorphology of Tidal Marshes*, Coastal and Estuarine Monograph Series, Vol. 59. Washington, D.C: American Geophysical Union, pp. 5–25.

Sorokin, P.Y., Sorokin, Y.I., Zakuskina, O.Y. & Ravagnan, G.P. (2002) On the changing ecology of Venice Lagoon. *Hydrobiologia*, 487(1), 1–18. Available from: https://doi.org/10.1023/A:1022939426396

Tagliapietra, D., Aloui-Bejaoui, N., Bellafiore, D., De Wit, R., Ferrarin, C., Gamito, S., Lasserre, P., Magni, P., Mistri, M., Pérez-Ruzafa, A., Pranovi, F., Reizopoulou, S., Rilov, G., Solidoro, C., Tunberg, B., Valiela, I. & Viaroli, P. (2011) The ecological implications of climate change on the lagoon of Venice. In: *The Future of Venice and its Lagoon in the Context of Global Change*. Venice: UNESCO, p. 45.

Tambroni, N. & Seminara, G. (2006) Are inlets responsible for the morphological degradation of Venice Lagoon? *Journal of Geophysical Research*, 111(F3), F03013. Available from: https://doi.org/10.1029/2005JF000334

Temmerman, S., Meire, P., Bouma, T.J., Herman, P.M.J., Ysebaert, T. & de Vriend, H.J.D. (2013) Ecosystem-based coastal defence in the face of global change. *Nature*, 504(7478), 79–83. Available from: https://doi.org/10.1038/nature12859

Toffolon, M. & Lanzoni, S. (2010) Morphological equilibrium of short channels dissecting the tidal flats of coastal lagoons. *Journal of Geophysical Research*, 115(F4), F04036. Available from: https://doi.org/10.1029/2010JF001673

Tognin, D., D'Alpaos, A., Marani, M. & Carniello, L. (2021) Marsh resilience to sea-level rise reduced by storm-surge barriers in the Venice Lagoon. *Nature Geoscience*, 14(12), 906–911. Available from: https://doi.org/10.1038/s41561-021-00853-7

Tommasini, L., Carniello, L., Ghinassi, M., Roner, M. & D'Alpaos, A. (2019) Changes in the wind-wave field and related salt-marsh lateral erosion: Inferences from the evolution of the Venice Lagoon in the last four centuries. *Earth Surface Processes and Landforms*, 44(8), 1633–1646. Available from: https://doi.org/10.1002/esp.4599

Tonelli, M., Fagherazzi, S. & Petti, M. (2010) Modeling wave impact on salt marsh boundaries. *Journal of Geophysical Research*, 115(C9), C09028. Available from: https://doi.org/10.1029/2009JC006026

Tosi, L., Teatini, P., Brancolini, G., Zecchin, M., Carbognin, L., Affatato, A. & Baradello, L. (2012) Three-dimensional analysis of the Plio-Pleistocene seismic sequences in the Venice Lagoon (Italy). *Journal of the Geological Society*, 169(5), 507–510. Available from: https://doi.org/10.1144/0016-76492011-093

Van Eerdt, R.R. (1985) Salt marsh cliff stability in the Oesterschelde, The Netherlands. *Earth Surface Processes and Landforms*, 10(2), 95–106. Available from: https://doi.org/10.1002/esp.3290100203

Wang, H., van der Wal, D., Li, X.Y., van Belzen, J., Herman, P.M.J., Hu, Z., Ge, Z.M., Zhang, L.Q. & Bouma, T.J. (2017) Zooming in and out: Scale dependence of extrinsic and intrinsic factors affecting salt marsh erosion. *Journal of Geophysical Research – Earth Surface*, 122(7), 1455–1470. Available from: https://doi.org/10.1002/2016JF004193

Young, I.R. & Verhagen, L.A. (1996) The growth of fetch limited waves in water of finite depth. Part 1. Total energy and peak frequency. *Coastal Engineering*, 29(1–2), 47–78. Available from: https://doi.org/10.1016/S0378-3839(96)00006-3

Zecchin, M., Brancolini, G., Tosi, L., Rizzetto, F., Caffau, M. & Baradello, L. (2009) Anatomy of the Holocene succession of the southern Venice Lagoon revealed by very high-resolution seismic data. *Continental Shelf Research*, 29(10), 1343–1359. Available from: https://doi.org/10.1016/j.csr.2009.03.006

How to cite this article: Mel, R.A., Bendoni, M. & Steffinlongo, D. (2022) Salt-marsh retreat on different time scales: Issues and prospects from a 5-year monitoring campaign in the Venice Lagoon. *Earth Surface Processes and Landforms*, 47(8), 1989–2005. Available from: https://doi.org/10.1002/esp.5359

APPENDIX A

Offshore and inshore wave power

Offshore wave power

Wave height H and wave period T in front of the bank have been computed by means of the Young and Verhagen model using observed sea level at Burano and wind speed and direction α_W gauged at San Giorgio and Laguna Nord (Figure 1). Wave height and wave period have been respectively corrected by the calibration coefficients 0.80 [see Equation 1] and 0.85 [see Equation 2] presented in the main text. Under the hypothesis of linear waves, we computed the angular frequency ω [Equation 3], the wavenumber k (deviation < 0.001) [Equation 4], the wave speed c [Equation 5], and the coefficient n [Equation 6], where h is the actual flow depth:

$$\omega = 2\frac{\pi}{T} \tag{3}$$

$$\frac{\omega^2}{g\tanh(kh)} = k \tag{4}$$

$$c_p = \frac{\omega}{k} \tag{5}$$

$$n = \frac{1}{2}\left[1 + \frac{2kh}{\sinh(2kh)}\right] \tag{6}$$

Assuming $\rho = 1025\ \mathrm{kg/m^2}$, we computed the wave energy E [Equation 7] and the (offshore) wave power P_O [Equation 8]:

$$E = \rho g\frac{H^2}{16} \tag{7}$$

$$P_O = E \cdot c_p \cdot n \tag{8}$$

Inshore wave power

For each transect i, we measured the elevation of the scarp top η_{TOP_i} and toe η_{TOE_i}, together with the angle perpendicular to the transect (α_{P_i}). The inshore wave power P_I is

$$P_I = P_O\cos(\alpha_W - \alpha_{P_i}) \tag{9}$$

Furthermore, the inshore wave power has been assumed not null only when both Equations (10) and (11) are verified:

$$\alpha_{P\_i} - 90^\circ < \alpha_W < \alpha_{P_i} + 90^\circ \tag{10}$$

$$\eta_{TOE\_i} < \mathrm{SL} < \eta_{TOP\_i} \tag{11}$$

We stress that for single surge surveys, we computed different values of wave power (and erosion rate accordingly) for the four elevations j of the pin rows. The domain of each pin row extends from 0.1 m below the pin to 0.1 m above the pin. Thus, for single surge analysis, Equation (11) becomes

$$\eta_j - 0.1\,\mathrm{m} < \mathrm{SL} < \eta_j + 0.1\,\mathrm{m} \tag{11.1}$$

APPENDIX B

The role of wave angle

To ascertain the best function to describe the wave power as a function of the angle α that waves form with the orientation of the marsh face, we compared the statistical parameters of the regression between wave power and erosion rate, by computing the wave power through three functions: cosine, quadratic, and constant (Figure B.1). The analysis has been performed on monthly data over the period 2014–2018.

If we compare the statistical parameters of the three linear regressions, we notice similar performances, with particular reference to the comparison between the cosine and the constant function (Table B.1). A possible explanation is the strong predominance of the northeastern winds (Figure B.1), which reduces the significance of the wind direction in accounting for wave power. Nevertheless, the correlation obtained through the cosine function provides statistical parameters that are marginally improved, confirming such a relationship suitable in accounting for the wave power, as assumed by Marani et al. (2011)).

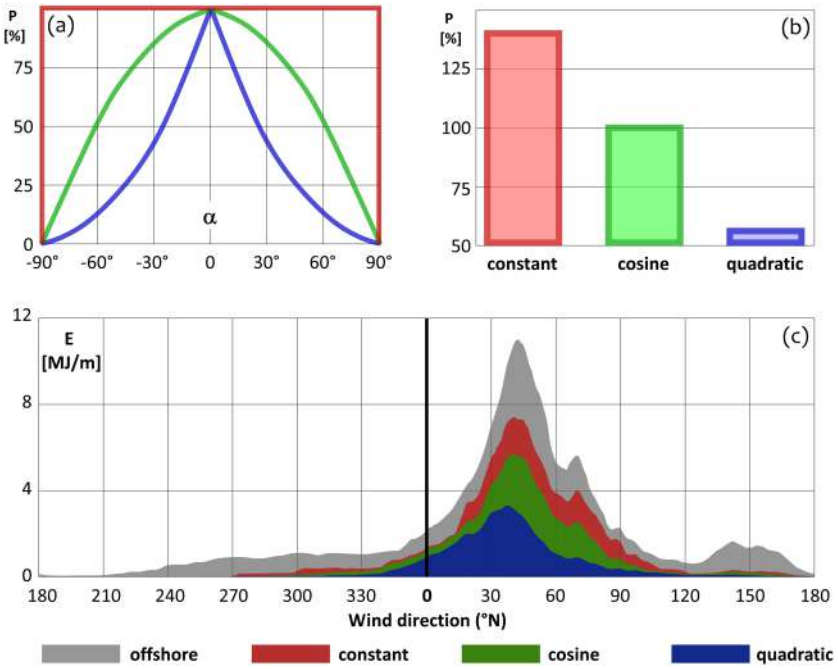

FIGURE B.1 Effect of different formulations in accounting for the wave power as a function of wave angle *a*, computed with respect to the perpendicular direction of the marsh bank: quadratic function (blue); cosine function used in this study (green); constant function (i.e. full wave power in the range $+90^{\circ}$ to -90°, red). (a) Representation of the three functions. (b) Wave power fraction compared to the cosine function. (c) 2014–2018 dataset. Wave energy flux offshore (grey) and impinging the marsh computed through the three functions [Color figure can be viewed at wileyonlinelibrary.com]

TABLE B.1 Linear regression of cosine, quadratic, and constant functions computed on the monthly data within the period 2014–2018. Statistical parameters are computed by aggregating the three transects. Grey-shaded cells denote the analysis performed if mass failures are not accounted for

Type of function	Slope	R^2	*p*-Value [5%]	RMSE data [m^2/yr]	RMSE slope [%]
Cosine	0.159	0.66	2.6×10^{-38}	0.502	5.8
Quadratic	0.278	0.63	4.9×10^{-36}	0.519	6.1
Constant	0.112	0.63	3.0×10^{-36}	0.518	6.0
Cosine	0.072	0.82	3.9×10^{-61}	0.146	3.7
Quadratic	0.124	0.77	1.1×10^{-52}	0.165	4.3
Constant	0.052	0.82	5.2×10^{-62}	0.144	3.6

APPENDIX C

Wind variability over the Venice Lagoon

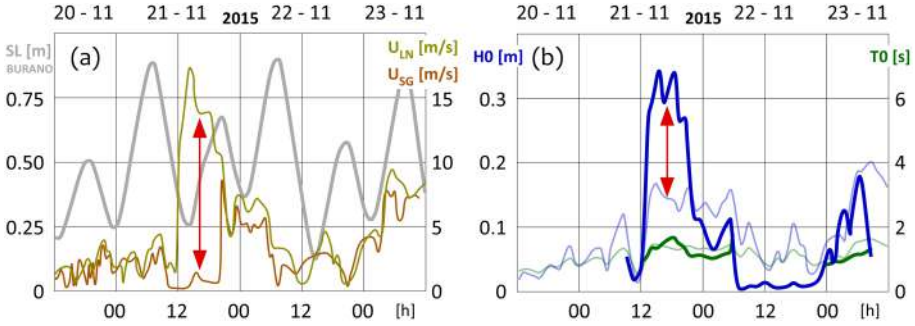

FIGURE C.1 Storm event of 20–23 November 2015. Faulty wind data gauged at San Giorgio led the wave forecast model to underestimate the wave height. Panel (a) shows the sea level at Burano (grey line) and the wind gauged at Laguna Nord (yellow) and San Giorgio (orange). Panel (b) compares the observed (dark lines) and computed (light lines) wave climate: blue lines represent the wave height; green lines the wave period [Color figure can be viewed at wileyonlinelibrary.com]

TABLE C.1 Dataset 2014–2018. Mean and quantiles of wind speed data (m/s; 5 s time step) among the CPSM gauges of Laguna Nord, San Giorgio, Malamocco Porto, Chioggia Porto, Diga Sud Lido, Diga Sud Chioggia, and CNR platform (Figure 1). Grey-shaded cells denote the seaward gauges

	Laguna Nord	San Giorgio	Mal. Porto	Chioggia Porto	Diga Sud Lido	Diga Sud Chioggia	CNR platform
Mean	3.5	3.5	4.1	4.0	4.2	3.9	4.9
Q > 90%	6.4	6.1	7.4	7.5	7.6	7.6	9.6
Q > 95%	7.9	7.4	8.9	9.2	9.6	9.4	12.2
Q > 98%	9.7	9.2	10.9	11.5	12.3	11.9	15.3
Q > 99%	11.1	10.5	12.2	13.4	14.2	13.4	17.3

TABLE C.2 Dataset 2014–2018. Absolute errors (Δ) frequency (%) computed on wind speed data (5 s time step) among the CPSM gauges. Wind speeds lower than 8 m/s have been excluded from this analysis. Values refer to the gauge labelled in red

Laguna Nord	San Giorgio	Mal. Porto	Chioggia Porto	Diga Sud Lido	Diga Sud Chioggia	CNR platform
Δ > 1 m/s	51.1	57.6	64.4	67.8	66.5	94.1
Δ > 2 m/s	21.5	28.5	39.5	50.2	43.1	85.7
Δ > 5 m/s	0.8	1.0	6.5	16.3	5.8	48.1
San Giorgio	Laguna Nord	Mal. Porto	Chioggia Porto	Diga Sud Lido	Diga Sud Chioggia	CNR platform
Δ > 1 m/s	51.1	71.2	79.7	73.4	77.5	94.5
Δ > 2 m/s	21.5	41.5	56.8	53.1	56.4	87.4
Δ > 5 m/s	0.8	2.0	9.8	19.7	8.7	54.0
Mal. Porto	Laguna Nord	San Giorgio	Chioggia Porto	Diga Sud Lido	Diga Sud Chioggia	CNR platform
Δ > 1 m/s	57.6	71.2	50.0	74.2	52.9	88.9
Δ > 2 m/s	28.5	41.5	20.3	50.4	22.1	76.6
Δ > 5 m/s	1.0	2.0	1.1	8.3	0.8	34.4
Chioggia Porto	Laguna Nord	San Giorgio	Mal. Porto	Diga Sud Lido	Diga Sud Chioggia	CNR platform
Δ > 1 m/s	64.4	79.7	50.0	68.6	29.7	89.9
Δ > 2 m/s	39.5	56.8	20.3	44.8	6.1	76.1
Δ > 5 m/s	6.5	9.8	1.1	7.5	0.0	22.9
Diga Sud Lido	Laguna Nord	San Giorgio	Mal. Porto	Chioggia Porto	Diga Sud Chioggia	CNR platform
Δ > 1 m/s	67.8	73.4	74.2	68.6	68.7	78.9
Δ > 2 m/s	50.2	53.1	50.4	44.8	45.0	60.4
Δ > 5 m/s	16.3	19.7	8.3	7.5	6.8	18.2
Diga Sud Chioggia	Laguna Nord	San Giorgio	Mal. Porto	Chioggia Porto	Diga Sud Lido	CNR platform
Δ > 1 m/s	66.5	77.5	52.9	29.7	68.7	87.3
Δ > 2 m/s	43.1	56.4	22.1	6.1	45.0	73.4
Δ > 5 m/s	5.8	8.7	0.8	0.0	6.8	20.8
CNR Platform	Laguna Nord	San Giorgio	Mal. Porto	Chioggia Porto	Diga Sud Lido	Diga Sud Chioggia
Δ > 1 m/s	94.1	94.5	88.9	89.9	78.9	87.3
Δ > 2 m/s	85.7	87.4	76.6	76.1	60.4	73.4
Δ > 5 m/s	48.1	54.0	34.4	22.9	18.2	20.8

TABLE C.3 Dataset 2014–2018. Linear regression parameters of wind speed data (5 s time step) among the CPSM gauges. Wind speeds lower than 8 m/s have been excluded from this analysis. Values refer to the gauge labelled in red

Laguna Nord	San Giorgio	Mal. Porto	Chioggia Porto	Diga Sud Lido	Diga Sud Chioggia	CNR platform
Slope	1.03	0.90	0.86	0.80	0.85	0.66
R^2	0.98	0.98	0.97	0.96	0.97	0.96
RMSE (m/s)	1.69	1.58	1.95	2.22	1.88	2.05
San Giorgio	Laguna Nord	Mal. Porto	Chioggia Porto	Diga Sud Lido	Diga Sud Chioggia	CNR platform
Slope	0.95	0.86	0.82	0.77	0.81	0.63
R^2	0.98	0.97	0.96	0.96	0.96	0.96
RMSE (m/s)	1.62	1.65	2.19	2.05	1.98	2.18
Mal. Porto	Laguna Nord	San Giorgio	Chioggia Porto	Diga Sud Lido	Diga Sud Chioggia	CNR platform
SlopeE	1.08	1.13	0.95	0.88	0.94	0.73
R^2	0.93	0.97	0.98	0.96	0.98	0.97
RMSE (m/s)	1.73	1.89	1.59	2.41	1.55	1.95
Chioggia Porto	Laguna Nord	San Giorgio	Mal. Porto	Diga Sud Lido	Diga Sud Chioggia	CNR platform
Slope	1.13	1.17	1.04	0.92	0.98	0.77
R^2	0.97	0.96	0.98	0.96	0.99	0.98
RMSE (m/s)	2.23	2.61	1.66	2.57	1.06	1.60
Diga Sud Lido	Laguna Nord	San Giorgio	Mal. Porto	Chioggia Porto	Diga Sud Chioggia	CNR platform
Slope	1.20	1.25	1.09	1.05	1.03	0.81
R^2	0.96	0.96	0.96	0.96	0.96	0.97
RMSE (m/s)	2.71	2.62	2.69	2.74	2.71	2.33
Diga Sud Chioggia	Laguna Nord	San Giorgio	Mal. Porto	Chioggia Porto	Diga Sud Lido	CNR platform
Slope	1.14	1.19	1.05	1.01	0.93	0.78
R^2	0.97	0.96	0.98	0.99	0.96	0.98
RMSE (m/s)	2.18	2.40	1.64	1.08	2.58	1.57
CNR platform	Laguna Nord	San Giorgio	Mal. Porto	Chioggia Porto	Diga Sud Lido	Diga Sud Chioggia
Slope	1.43	1.51	1.33	1.28	1.19	1.27
R^2	0.96	0.96	0.97	0.98	0.97	0.98
RMSE (m/s)	3.02	3.37	2.64	2.07	2.82	2.00